Acta Cryst. (1992). A**48**, 596-610

Relationship Between Lorentz Factor and Peak Width. Development of a New Peak-Width Formula and a Generalized Lorentz Factor for Single and Multiple Diffraction

BY ELISABETH ROSSMANITH

Mineralogisch-Petrographisches Institut der Universität Hamburg, D-2000 Hamburg 13, Grindelallee 48, Germany

(*Received* 19 *July* 1991; *accepted* 15 *January* 1992)

Abstract

While, in conventional Bragg scattering experiments, the Bragg angle is rarely smaller than 5° or greater than 75°, angles making the standard peak-width formula and the Lorentz factor extremely high or even infinite are neither impossible nor unusual in multiple-diffraction experiments. In the computer program *UMWEG*90, which can be used in all experimental situations, other expressions - valid for all possible experimental conditions - have therefore to be used. It is shown that the Lorentz factor for single diffraction can be expressed as a function of the width of the intensity profiles $\Delta\theta_h$, obtained in the $\theta/2\theta$-scan mode, and of the 'effective thickness' l of the Ewald sphere in the direction of the reflected X-ray beam. New formulae for both these quantities, $\Delta\theta_h$ and l, are derived. It is shown that the peak width of the intensity profiles and the 'effective thickness' of the Ewald sphere can be calculated in a simple manner from the divergence δ and the wavelength spread $\Delta\lambda/\lambda$ of the incident beam and from the mosaic spread η and the magnitude r of the ideally perfect crystallites in the sample. Moreover, it is shown that the new Lorentz factor, $L = \Delta\theta_h/(l\lambda)$, is equivalent to the familiar one, except for Bragg angles in the vicinity of zero and $\pi/2$. In the next step, formulae for the two peak-width and Lorentz factors, $\Delta\theta_{Umweg}$, L_θ for the θ rotation and $\Delta\psi_{Umweg}$, L_ψ for the ψ rotation, involved in the double-diffraction process, are developed. Lastly, it is shown that, using the new formulas introduced in this paper, an excellent agreement is obtained between calculated and measured *Umweganregung* patterns of the forbidden 003 reflection of Zn as well as the 'almost forbidden' 222 reflection of diamond, indicating that *UMWEG*90 is an efficient tool for the characterization of the incident beam as well as the mosaic structure of the crystal.

I. Introduction

During a ψ scan (Renninger, 1937), the crystal is rotated about the normal to the reflecting plane whose Bragg intensity is measured. In the θ-2θ-ψ-scan technique, for each step in ψ, a $\theta/2\theta$ scan is performed. In Fig. 1(*a*) the three-dimensional plot of a measured θ-2θ-ψ scan is given. Details about the experimental conditions are summarized in Rossmanith (1986). The intensity of the forbidden 003 reflection of Zn is plotted *vs* θ and ψ, showing prominent peaks that are due to multiple diffraction. In the Renninger experiment, the entire peak intensity in θ is not measured; only a relatively small θ region in the vicinity of the maximum of the peak is recorded using the counter.

Multiple diffraction occurs if at least three reciprocal-lattice points lie simultaneously on the Ewald sphere: the zero point, O, of the lattice, the point B belonging to the primary reflection $\mathbf{h}_{prim}$ and the point O' belonging to the operative reflection $\mathbf{h}_{op}$. In Fig. 2, the experimental conditions in reciprocal space are shown. The intensity of the X-ray beam, incident parallel to $\mathbf{s}_0$, is diffracted in the $\mathbf{s}_1$ as well as in the $\mathbf{s}_2$ direction. The reflected intensity in the $\mathbf{s}_2$ direction behaves as incident intensity for the cooperative reflection $\mathbf{h}_{coop}$, which reflects part of this intensity in the direction $\mathbf{s}_1$. This is the so-called *Umweganregung* effect.

It is obvious from Fig. 1(*a*) that the 'integrated intensity' of an *Umweganregung* event depends on both the rotation about the θ axis of the primary reflection $\mathbf{h}_{prim}$ (see Fig. 2) and the rotation about the ψ axis, which is parallel to the scattering vector $\mathbf{h}_{prim}$. Two Lorentz factors - L_θ and L_ψ - have therefore to be considered in the kinematical expression of the 'integrated intensity' of an *Umweganregung* event

$$\mathbf{I}_{Umweg} = \text{scal} \times p_{12} L_\theta L_\psi F_{op}^2 F_{coop}^2, \qquad (1a)$$

where scal is a scale factor and p_{12} is the polarization factor for the *Umweganregung* event given by Zachariasen (1965) and F_{op}, F_{coop} are the structure factors of the operative and cooperative reflections respectively.

Integrating the measured intensity, shown in Fig. 1(*a*), with respect to θ and plotting it against ψ results in the so-called *Umweganregung* pattern, which is shown in Fig. 1(*b*). With the help of the program *UMWEG*90, the profiles of this pattern can be calculated for each step in ψ (Fig. 1*c*). For this purpose, it is assumed that the intensity profile of each

0108-7673/92/040596-15$06.00

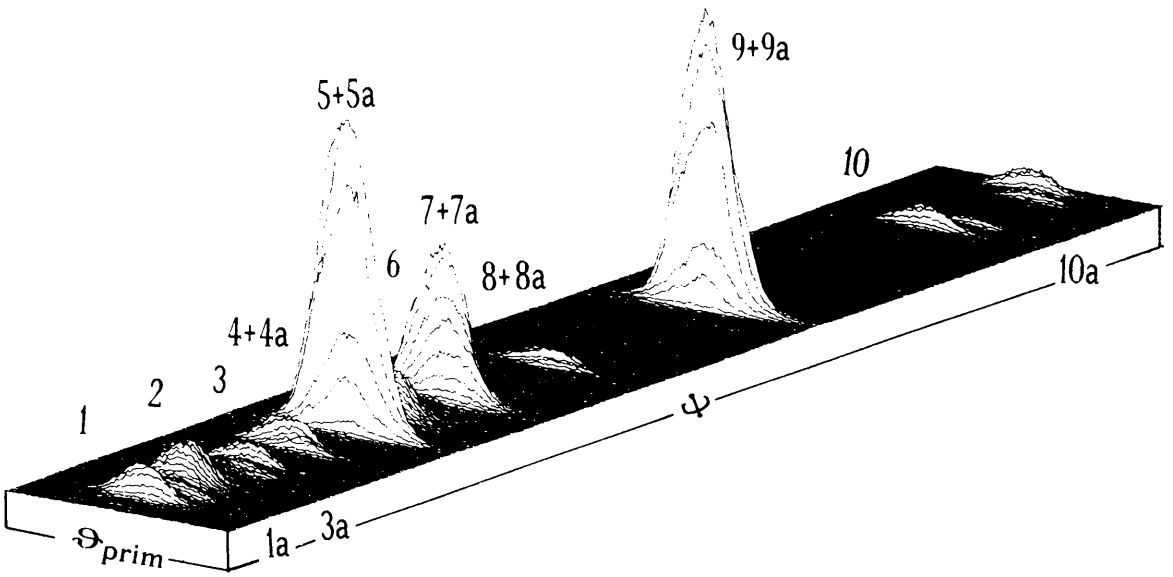

(a)

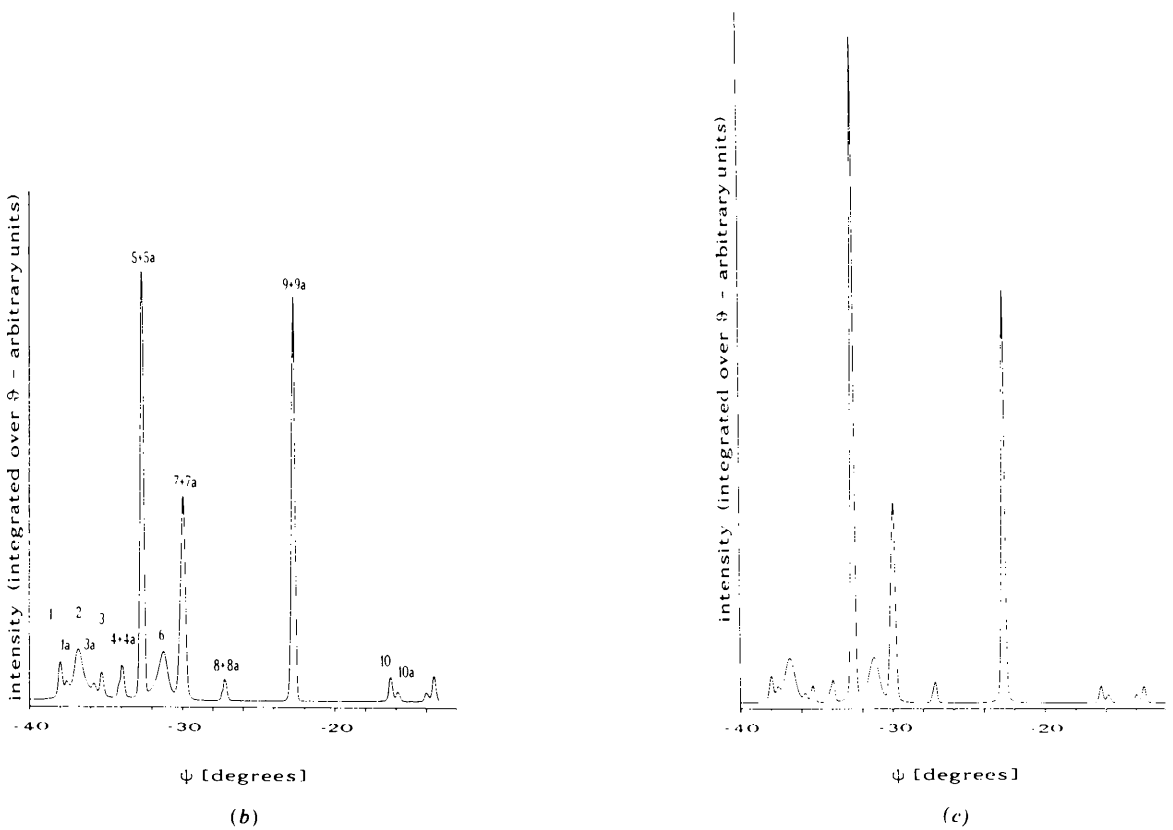

(b) (c)

Fig. 1. The forbidden 003 reflection of Zn. (*a*) Three-dimensional plot of the measured θ-2θ-ψ scan. Cu $K\alpha$; $\theta_{prim} = 27.57$ to $28.29°$; $\theta_{prim}(K\alpha_1) = 27.89°$; $\theta_{prim}(K\alpha_2) = 27.96°$; $\psi = -39$ to $-12°$. Peaks 1 to 10 due to Cu $K\alpha_1$, 1*a* to 10*a* due to Cu $K\alpha_2$. (*b*) Measured *Umweganregung* pattern. Intensities of (*a*), integrated over the θ scans, *vs* ψ. $\psi = -40$ to $-13°$. Peaks 1 to 10 due to Cu $K\alpha_1$, 1*a* to 10*a* due to Cu $K\alpha_2$. (*c*) *Umweganregung* pattern calculated with *UMWEG*90. Space group: $P6_3/mmc$; atomic positions: $\pm(\frac{1}{3}, \frac{2}{3}, \frac{1}{4})$; temperature parameters: $\beta_{11} = \beta_{22} = 0.03796$, $\beta_{33} = 0.020607$, $\beta_{12} = \beta_{11}/2$, $\beta_{13} = \beta_{23} = 0$; GL = 0.15; atomic scattering factors for Zn^{2+}: Table 2.2*B*, *International Tables for X-ray Crystallography* (1974); remaining parameters used are given in the heading of Table 1.

Umweganregung peak with respect to the azimuthal angle ψ can be approximated by the use of a normalized Gaussian distribution

$$[(2\pi)^{1/2}\sigma_{op}]^{-1}\int \exp\{-\tfrac{1}{2}(\psi-\psi_{op})^2/\sigma_{op}^2\}\,d\psi = 1. \quad (1b)$$

Consequently, the intensity $I(\psi_i)_{op}$ for each step ψ_i is given by

$$I(\psi_i)_{op} = \text{scal} \times p_{12} L_\theta L_\psi F_{op}^2 F_{coop}^2 [(2\pi)^{1/2}\sigma_{op}]^{-1} \times \exp\{-\tfrac{1}{2}(\psi_i-\psi_{op})^2/\sigma_{op}^2\}. \quad (1c)$$

Because of possible overlapping of different *Umweganregung* peaks at a particular azimuthal angle ψ_i of the ψ scan, the total intensity at that particular ψ_i is given by

$$I(\psi_i) = \sum_{op} f(\alpha_{1,2}) I(\psi_i)_{op}, \quad (1d)$$

where $f(\alpha_{1,2})$ depends on the intensity ratio of the $K\alpha_1$ and $K\alpha_2$ radiation.

In the classical Renninger experiment, the intensity of the multiple-scattering events as a function of the azimuthal angle ψ for constant $\theta = \theta_{prim}$ is measured. In analogy to (1*c*), the intensity in this case is given by

$$I(\psi_i)_{op} = \text{scal} \times p_{12} L_\theta L_\psi F_{op}^2 F_{coop}^2 (8\ln 2)^{1/2} \times [(2\pi)^{1/2}\Delta\theta_{Umweg}]^{-1}[(2\pi)^{1/2}\sigma_{op}]^{-1} \times \exp\{-\tfrac{1}{2}(\psi_i-\psi_{op})^2/\sigma_{op}^2\}, \quad (1e)$$

where $\Delta\theta_{Umweg}$ is the full width at half-maximum (FWHM) of the intensity profiles of the $\theta/2\theta$ scan.

It is straightforward to calculate the angles in the peak maxima, the structure factors and the polarization factor. The problem is to find expressions for the peak widths and Lorentz factors, applicable to all possible experimental conditions in multiple-scattering experiments.

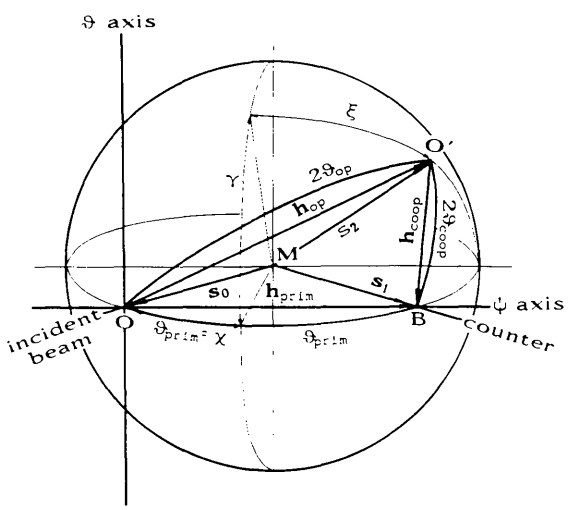

Fig. 2. The geometry of multiple diffraction in reciprocal space.

In § II it will be shown that both the peak widths and the Lorentz factors can be expressed as functions of the wavelength spread and divergence of the incident beam and the mosaic structure of the crystal. The fundamentals of the derivation for single and multiple diffraction in the framework of the kinematical theory will be given in §§ II.*A* and II.*B* respectively. Following the recommendation of one of the referees, the detailed formulae will not be given here.

II. Theory: relationship between the peak width and the Lorentz factor

A. The 'integrated intensity' obtained during a $\theta/2\theta$ scan

In § II*A* the considerations will, for simplicity, be confined to the 'integrated intensity' of a Bragg reflection measured in the $\theta/2\theta$-scan technique. In this technique, the crystal and the receiver are rotated about an axis perpendicular to the incident and reflected beams. The motion of the crystal and receiver are coordinated with respective velocities $\dot\theta$ and $2\dot\theta$. The geometrical conditions of the measurement in reciprocal space are given in Figs. 3(*a*)-(*d*).

1. *Proposal for a new peak-width formula*

Dependence of the peak width on the radius of the ideally perfect crystallites. It will be assumed at first that the incident beam is exactly parallel and monochromatic and that the crystal is ideally perfect.

The ideally perfect crystal is assumed, for simplicitly, to be spherical with radius r. For an arbitrary reflection **h**, the radius r can be expressed as $d_{\mathbf{h}}N_{\mathbf{h}}$, where $d_{\mathbf{h}}$ is the interplanar spacing of the reflecting planes and $2N_{\mathbf{h}}$ is the number of planes in the sphere. From the construction of the reciprocal space it follows that $d_{\mathbf{h}}$ is represented in reciprocal space by a vector **h** normal to the reflecting planes, with length $1/d_{\mathbf{h}} = d_{\mathbf{h}}^*$ and consequently any ray from the origin with length r in direct space is represented by a vector parallel to this ray with length $1/r = \varepsilon$ in reciprocal space. In the direction **h**, the value of ε is given by $\varepsilon = 1/(N_{\mathbf{h}}d_{\mathbf{h}}) = d_{\mathbf{h}}^*/N_{\mathbf{h}}$. Because of the finite number $N_{\mathbf{h}}$ of planes in the sample, the zero point O of the reciprocal lattice is enlarged to a sphere with radius ε and becasue of the constant distance $d_{\mathbf{h}}^*$ between the 'origin' and the 'point' **h** in the reciprocal lattice, enlargement of the 'zero point' results in the equivalent enlargement of the 'point' **h** in the reciprocal lattice. The lattice 'points' are dimensionless mathematical points only in the case $N_{\mathbf{h}} = \infty$. An ideally perfect crystal sphere with radius r is therefore represented in reciprocal space by the replacement of the lattice 'points' by lattice spheres with radius $\varepsilon = 1/r$.

In the reciprocal space, the rotation of the crystal about the θ axis is represented as a rotation of all

'lattice spheres' about the origin of the lattice. Significant intensity of the Bragg reflection will be observed in the counter (Fig. 3*a*) as long as the 'lattice sphere' passes the Ewald sphere. P_2-P_1 in Fig. 3(*a*) is the trajectory of the centre of the 'reciprocal-lattice sphere' P during rotation of the crystal about the θ axis. At P', the 'lattice sphere' first touches the Ewald sphere and P'' is the point of last contact with the Ewald sphere during rotation. The peak width $\Delta\theta_h$ of the reflection **h** is given by the angle P_1OP_2

$$\Delta\theta_h(\varepsilon) = \delta_2 - \delta_1 \qquad (2a)$$

with

$$\delta_{2,1} = \cos^{-1}\{[r^{*2} + d_h^{*2} - (r^* \pm \varepsilon)^2]/(2r^* d_h^*)\} \qquad (2b)$$

(consider the triangles OMP_1 and OMP_2), where $r^* = 1/\lambda$ and λ is the wavelength of the X-ray. The same peak width is obtained using an alternative picture, in which lattice points pass a 'thick' Ewald sphere, which consists of two spheres denoted $S1$ and $S2$ with the same centre M, but with different radii $r^* - \varepsilon$ and $r^* + \varepsilon$.

From Fig. 3(*a*) it is obvious that $\Delta\theta_h(\varepsilon)$ can be calculated approximately using the relations

$$b = \Delta\theta_h(\varepsilon) d_h^* = \Delta\theta_h(\varepsilon) 2(\sin\theta_h)/\lambda, \qquad (3a)$$

where b is the arc P_1P_2 and (consider triangle $PP'P_2$)

$$b \sim 2\varepsilon/(\cos\theta_h). \qquad (3b)$$

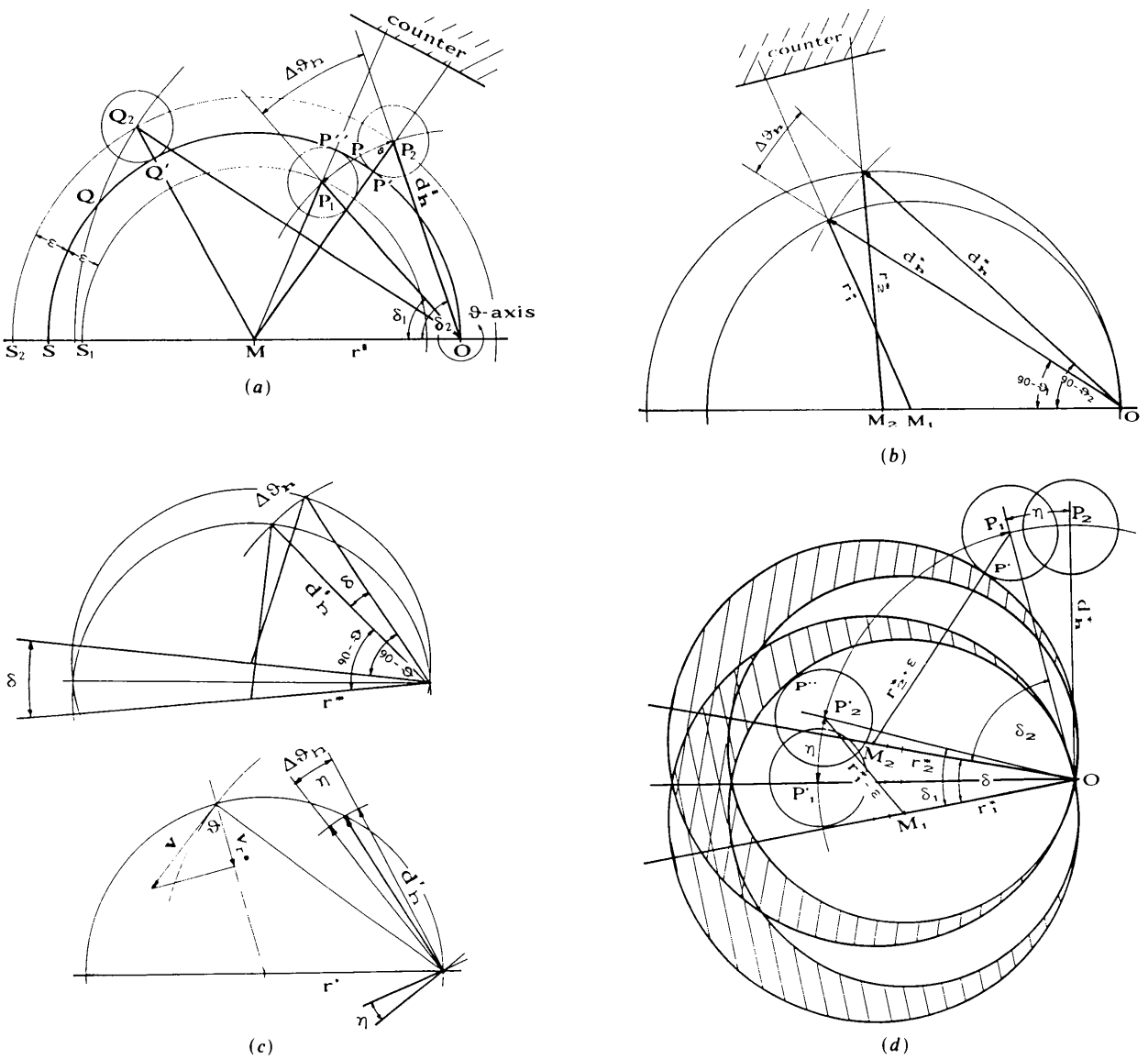

Fig. 3. Dependences of the peak width: (*a*) on the radius r of an ideally perfect crystal sphere; (*b*) on the wavelength spread $\Delta\lambda/\lambda$; (*c*) on the beam divergence δ and the crystal mosaic spread η. (*d*) The peak width $\Delta\theta_h$ in a real experiment.

Table 1. *Peak width $\Delta\theta_h$ in degrees calculated for* Cu $K\alpha_1$ *radiation*

$r = 1/\varepsilon = 1.5$ μm; $\Delta\lambda/\lambda = 0.000306$; $\delta + \eta = 0.116°$.

θ_h	$\Delta\theta_h(\varepsilon)$ (2a, b)	$\Delta\theta_h(\lambda)$ (4a)	(4b)	$\Delta\theta_h$ (6a)	(6b)
0.2	1.686	0.000	0.000	1.802	0.128
0.6	0.562			0.678	
1.0	0.337			0.454	
1.4	0.241			0.357	
5.0	0.068	0.002	0.002	0.185	0.130
15.0	0.024	0.005	0.005	0.144	0.133
25.0	0.015	0.008	0.008	0.140	0.136
35.0	0.013	0.012	0.012	0.141	0.140
45.0	0.012	0.018	0.018	0.145	0.146
55.0	0.013	0.025	0.025	0.154	0.153
65.0	0.015	0.038	0.038	0.169	0.166
75.0	0.024	0.065	0.065	0,205	0.193
85.0	0.068	0.200	0.200	0.384	0.328
88.2	0.188	0.565	0.558	0.879	0.686
88.4	0.211	0.641	0.628	0.987	0.756
88.6	0.242	0.744	0.717	1.147	0.845
88.8	0.283	0.903	0.837	1.470	0.965
89.0	0.342	2.832	1.004	3.177	1.132
89.2	0.438	2.565	1.256	2.932	1.384
89.4	0.684	2.336	1.674	2.725	1.802
89.6	1.410	2.158	2.511	2.567	2.639
89.8	1.228	2.044	5.023	2.467	5.151
90.0	1.161	2.005	∞	2.433	∞

From triangle $QQ'Q_2$ it is evident that (3*b*) is approximately valid only for intermediate angles θ. Combination of (3*a*) and (3*b*) results in

$$\Delta\theta_h(\varepsilon) \sim 2\varepsilon\lambda/[2(\sin\theta)(\cos\theta)] = (2/r)\lambda/(\sin 2\theta), \quad (3c)$$

which bears some similarity to the peak width deduced in the framework of the dynamical theory for a thin plane parallel crystal plate (Zachariasen, 1945, formula 3.159).

In the second column of Table 1, the peak width (2*a*) calculated for a perfect-crystal sphere with radius $r = 1/\varepsilon = 1.5$ μm and Cu $K\alpha_1$ radiation is given. In contrast to formula (3*c*), formula (2*a*) results in finite peak width over the whole range of θ. In contrast to the Scherrer formula used in powder diffractometry, it predicts a broadening effect due to the particle-size effect not only for large but also for small values of θ.

Dependence of the peak width on the wavelength spread of the incident beam. The influence of the wavelength spread $\Delta\lambda = \lambda_1 - \lambda_2$ on $\Delta\theta_h$, for the case of an infinite ideally perfect crystal ($\varepsilon \sim 0$) and an exactly parallel incident beam, is depicted in Fig. 3(*b*). Two limiting Ewald spheres with $r_1^* = 1/\lambda_1 = 1/(\lambda + \Delta\lambda/2)$ and $r_2^* = 1/\lambda_2 = 1/(\lambda - \Delta\lambda/2)$ pass through the origin of the reciprocal lattice. Significant intensity of the Bragg reflection will be recorded on the counter as long as the lattice point passes the region between the two limiting Ewald spheres during rotation about the origin of the lattice. It can be easily deduced from Fig. 3(*b*) that $\Delta\theta_h(\lambda)$ is given by

$$\Delta\theta_h(\lambda) = \theta_1 - \theta_2, \quad (4a)$$

where θ_1 and θ_2 are the Bragg angles for λ_1 and λ_2 respectively.

In the third and fourth column of Table 1, the peak width defined in (4*a*) is compared with results for the commonly used formula

$$\Delta\theta_h(\lambda) = (\Delta\lambda/\lambda)\tan\theta_h. \quad (4b)$$

For $\Delta\lambda$ the value given by Ladell, Zagofsky & Pearlman (1975) for Cu $K\alpha_1$ was used. Apart from a θ range near $\theta = \pi/2$, both columns are identical. For $\theta = \pi/2$, $\Delta\theta_h(\lambda)$ defined in (4*b*) becomes infinite and therefore cannot be used as approximation in the vicinity of $\pi/2$. $\Delta\theta_h(\lambda)$ defined in (4*a*), on the other hand, is finite everywhere. The maximum at $\theta = 89.0$ is easily understood from Fig. 3(*b*).

Dependence of the peak width on the mosaic spread of the crystal and on the divergence of the incident beam. The factors influencing the geometrical line width sum up to the divergence δ of the incident beam. As can be deduced from Fig. 3(*c*), the influence of the divergence δ and mosaic spread η on $\Delta\theta_h$ does not depend on θ_h. In the case $\varepsilon \sim 0$, $\Delta\lambda \sim 0$ and $\eta \sim 0$, $\Delta\theta_h(\delta)$ is given by δ for all θ_h, and in the case $\varepsilon \sim 0$, $\Delta\lambda \sim 0$ and $\delta \sim 0$, $\Delta\theta_h(\eta)$ is given by η. In the case where both δ and η are nonzero, the two components cannot be distinguished. δ and η add up to a final peak width, constant for all θ,

$$\Delta\theta_h(\delta + \eta) = \delta + \eta. \quad (5)$$

The peak width in a real experiment. In practice, $\Delta\theta_h$ depends on all the quantities ε, η, $\Delta\lambda$ and δ simultaneously, all four being zonzero. In this case, $\Delta\theta_h$ can be determined approximately using Fig. 3(*d*). The limiting Ewald spheres, due to the divergence δ, are broadened, due to the wavelength spread $\Delta\lambda$. The 'reciprocal-lattice sphere' P_1 is for the first time in a reflection position at P' and the 'reciprocal-lattice sphere' P_2 is for the last time in a reflection position at P''. The peak width $\Delta\theta_h$ is therefore given by the angle P_1OP_1'. It is obvious from Fig. 3(*d*) that

$$\Delta\theta_h = \delta_2 + \delta - \delta_1 + \eta. \quad (6a)$$

δ_1 and δ_2 can easily be obtained from the triangles OM_1P_2' and OM_2P_1 in analogy to (2*b*). It is therefore not at all difficult to calculate the peak width defined in (6*a*) with the help of a computer. In Table 1, the peak width (6*a*) is compared with the peak widths

$$\Delta\theta_h = \text{constant} + (\Delta\lambda/\lambda)\tan\theta_h, \quad (6b)$$

which is normally used for $\theta/2\theta$-scan-range calculations in diffractometry using conventional X-ray tubes [see for example Furnas (1957) or the manual of the single-crystal diffractometer CAD-4 by Enraf–Nonius (1982)]. For the constant term in (6*b*), the value 0.128° [$\equiv \Delta\theta_h(\varepsilon)_{45} + (\delta + \eta) = 0.012 + 0.116°$] was used.

Columns five and six of Table 1 show similar values only in the θ region between 15 and 75°, where they differ by less than 0.012°. For θ less than 15°, the peak width is slowly decreasing according to (6*b*), whereas a peak broadening due to the particle-size effect is obtained with (6*a*). For θ greater than 75°, the two columns differ appreciably. The steeper increase of $\Delta\theta_h$ due to (6*a*) levels off at a finite value, whereas (6*b*) becomes infinite at $\theta = 90°$. In (6*b*), the term due to the wavelength spread is dominant. The peak width calculated with (6*a*), on the other hand, is finite in the whole range of θ. The maximum at 89.0° can be easily understood from Fig. 3(*d*).

In Fig. 4, the peak width calculated with (6*a*) and (6*b*) respectively are compared with experimental values. The full width at half-maximum (FWHM) values for the Cu $K\alpha_1$ component have been estimated from the step-scan profiles of Bragg reflections measured in the $\theta/2\theta$ mode with Cu $K\alpha$ radiation using a Zn single-crystal sphere with diameter 100 μm (Bengel, 1991). The two theoretical peak widths, calculated using the input parameters given in the heading of Table 1, deviate only slightly for the θ range of the measurement, the main difference being the minimum of the peak width calculated with (6*a*) at about $\theta = 26°$. The main advantage of the new formula is that it is entirely calculated from physically meaningful parameters. The significance of the new peak-width formula will be discussed further in § *B*, where multiple scattering is considered.

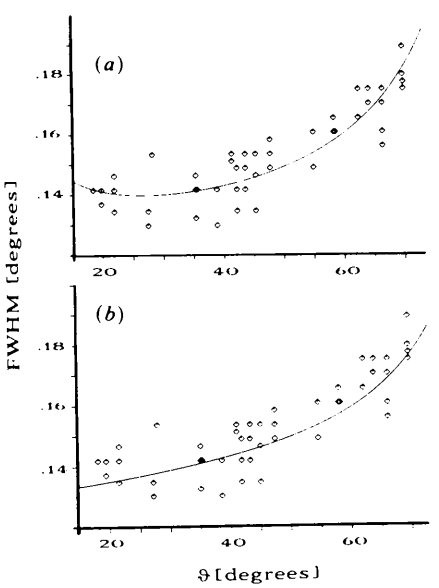

Fig. 4. Comparison of measured and calculated peak width $\Delta\theta_h$ of Zn. Symbol ◇: peak width (FWHM) for Cu $K\alpha_1$ deduced from measurement with Cu $K\alpha$ radiation. (*a*) Theoretical curve calculated with (6*a*). Input parameters for calculation as in the heading of Table 1. (*b*) Theoretical curve calculated with (6*b*). Constant term in (6*b*) is 0.128°.

2. *Proposal for a generalized Lorentz factor*

The intensity of coherent scattering of an exactly monochromatic and parallel incident beam from an ideally perfect small crystal

$$I_{coh}^{ideal} = I_e |F_h|^2 G^2 \qquad (7a)$$

is negligible unless Bragg's law is exactly or very nearly satisfied (Compton & Allison, 1935; Zachariasen, 1945; James, 1948; Buerger, 1960; Laue, 1960; Azaroff, 1968; Wölfel, 1975). The scattered intensity is proportional to the well known interference function G^2 of the kinematical approach and is therefore a function of the scattering angle θ. The exceedingly sharp function G^2 has its maximum at $\theta = \theta_h$, where θ_h is the Bragg angle. The peak height is proportional to the square of the number of unit cells in the crystal,

$$(I_{coh}^{ideal})_{max} = I_e |F_h|^2 (V_{cry}/V_{cell})^2, \qquad (7b)$$

its tiny but finite half width is inversely proportional to the number of unit cells N_h in the direction $\mathbf{h}$ involved in the scattering process. I_e is the intensity scattered by an electron and F_h is the structure factor. I_e and F_h are both slowly varying functions of θ and are therefore usually assumed to be constant in the region of θ, where G^2 is significantly greater than zero. V_{cry} and V_{cell} are the volumes of the crystal and the unit cell respectively.

In practice, the crystal is not ideally perfect and the incident beam is neither ideally monochromatic nor are the rays of the beam exactly parallel. Experimentally, one cannot therefore measure the intensity (7*b*) for a sharply defined scattering direction, so an average intensity for scattering directions lying within a finite solid angle is measured. The measurement corresponds to an integration

$$\int I_{coh}^{ideal}\, d\mathbf{x} = I_e |F_h|^2 \int G^2\, d\mathbf{x} = \mathbf{I}_h \qquad (7c)$$

and $\mathbf{I}_h$ is therefore commonly called the 'integrated intensity'. The variable $\mathbf{x}$ depends on the experimental conditions.

For the rotating-crystal method, the 'integrated intensity' of the single Bragg reflection $\mathbf{I}_h$ is given by (Azaroff, 1968, p. 199)

$$\mathbf{I}_h = (R^2/\omega) I_e |F_h|^2 (V_{cry}/V_{cell})^2 L(\lambda^3/V_{cry}), \qquad (7d)$$

where R is the distance between the scattering electrons and the counter and ω is the uniform angular velocity of the crystal rotation. L is the Lorentz factor and λ is the wavelength of the radiation used for diffraction. The 'integrated intensity' $\mathbf{I}_h$ is the energy received by the counter during rotation of the crystal.

For a crystal rotation about an arbitrary axis, Zachariasen (1945) has given for the Lorentz factor L the expression (his formula 3.78)

$$L = 1/(\sin\gamma \cos\chi \cos\xi). \qquad (8a)$$

The angles involved in (8*a*) are defined Fig. 2 with respect to the ψ axis.

When the crystal is rotated about an axis normal to the incident and reflected beams ($\xi = \chi = 0$), as in the usual rocking curve or $\theta/2\theta$-scan experiments, the Lorentz factor (8*a*) reduces to the familiar expression

$$L = 1/\sin 2\theta_{\mathbf{h}}. \qquad (8b)$$

A lot of approximations are necessary to yield the 'integrated intensity' in the simple form given in formula (7*d*). Different approaches to achieve the desired result (7*d*) in connection with (8*a*) or (8*b*) can be found in the literature. Because of the approximations used, the Lorentz factors defined in (8*a*) and (8*b*) are not valid for all possible experimental conditions, being infinite for special angles and resulting in an infinite scattered intensity for the corresponding reflections. These Lorentz factors cannot therefore be used in computer programs applied to all experimental situations. The derivation of the Lorentz factor given by Laue (1960) was therefore reconsidered using the geometrical constructions of Figs. 2 and 3(*a*)-(*d*).

Dependence of the Lorentz factor on the radius of the ideally perfect crystallites. Again, it will first be assumed that the incident beam is exactly parallel and monochromatic and that the crystal is ideally perfect.

For the rotating-crystal method, the 'integrated intensity' $\mathbf{I}_{\mathbf{h}}$, detected by the counter, is given by (Laue,1960, p. 199)

$$\mathbf{I}_{\mathbf{h}} = (R^2/\omega) I_e |F_{\mathbf{h}}|^2 \int\int G^2 \, \mathrm{d}\theta \, \mathrm{d}\Omega, \qquad (9a)$$

where the solid angle $\mathrm{d}\Omega$ in the direction of the diffracted beam as well as a small element of rotation about the θ axis, $\mathrm{d}\theta$, are represented in Fig. 5(*a*). Moreover, in Fig. 5(*a*) the volume element in reciprocal space, $\mathrm{d}V^*$, is represented by the area element $\mathrm{d}S$, perpendicular to the reflected beam, and the element $\mathrm{d}l$ in the direction of the reflected beam,

$$\mathrm{d}V^* = dS \, \mathrm{d}l. \qquad (9b)$$

It is obvious from Fig. 5 that the reciprocal-lattice point P_1 moves a distance $l = P_1M - P_2M = 2\varepsilon$ against the direction of the reflected beam during the rotation $\Delta\theta_{\mathbf{h}}(\varepsilon)$ about the θ axis and that $\mathrm{d}l$ corresponds to the distance between two consecutive intersecting areas S and S' of the 'lattice sphere' with the Ewald sphere before (S) and after (S') rotating the crystal $\mathrm{d}\theta$ degrees (see Fig. 5*a*). l is the 'effective thickness' of the Ewald sphere in the direction of the reflected beam. From Fig. 5(*a*), the two equations

$$\mathrm{d}l : 2\varepsilon = \mathrm{d}\theta : \Delta\theta_{\mathbf{h}}(\varepsilon) \qquad (9c)$$

and

$$\mathrm{d}S = (1/\lambda^2) \, \mathrm{d}\Omega \qquad (9d)$$

can easily be deduced. Thus the relation

$$\int\int G^2 \, \mathrm{d}\theta \, \mathrm{d}\Omega = \lambda^2 [\Delta\theta_{\mathbf{h}}(\varepsilon)/(2\varepsilon)] \int G^2 \, \mathrm{d}V^* \qquad (9e)$$

is obtained. From the relation (Laue, 1960, p. 191)

$$\int G^2 \, \mathrm{d}V^* = V_{\mathrm{cry}}/V_{\mathrm{cell}}^2, \qquad (9f)$$

the integration in (9*a*) can easily be performed. The 'integrated intensity' can therefore be expressed as

$$\mathbf{I}_{\mathbf{h}} = (R^2/\omega) I_e |F_{\mathbf{h}}|^2 V_{\mathrm{cry}}/V_{\mathrm{cell}}^2 \lambda^2 \Delta\theta_{\mathbf{h}}(\varepsilon)/(2\varepsilon). \qquad (9g)$$

$\Delta\theta_{\mathbf{h}}(\varepsilon)$ is defined in (2*a*). By comparison of (7*d*) with

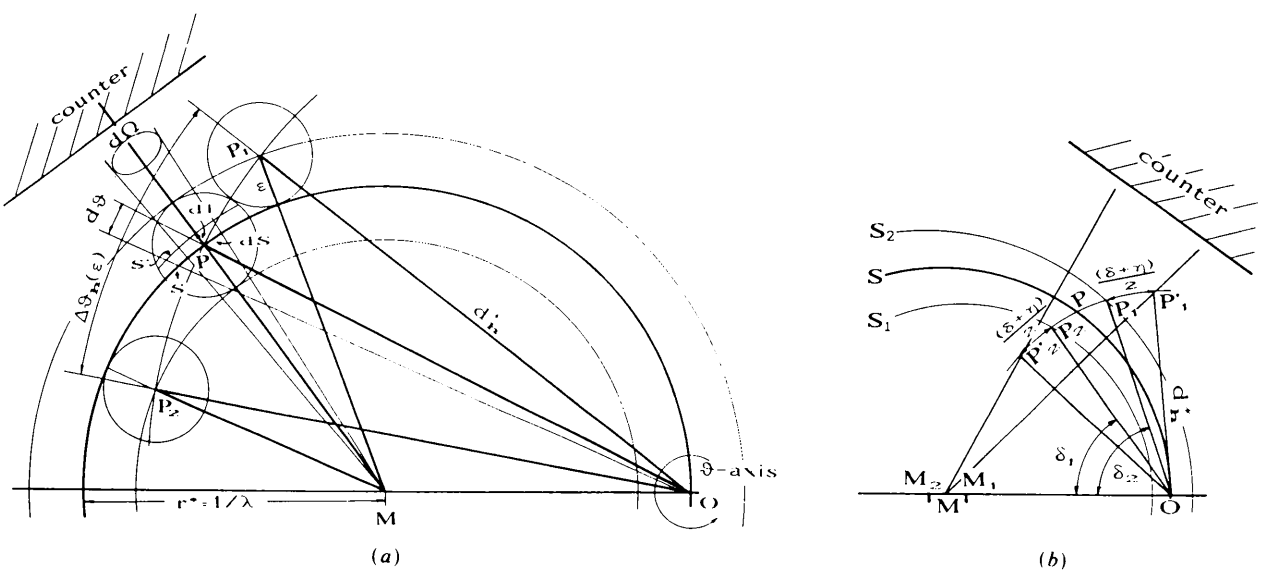

Fig. 5. (*a*) Derivation of the Lorentz factor for an ideally perfect crystal sphere. (*b*) The 'effective thickness' of the Ewald sphere in a real experiment.

Table 2. *Lorentz factor L and 'effective thickness' l of the Ewald sphere calculated for* Cu $K\alpha_1$ *radiation*

$r = 1/\varepsilon = 1.5$ μm; $\Delta\lambda/\lambda = 0.000306$; $\delta + \eta = 0.116°$. Columns six and seven are the results of calculations using these parameters; for comparison, columns four and five give the appropriate values for $\varepsilon = \eta = \delta = 0$.

θ_h	L (8*b*)	$L(\varepsilon)$ (9*h*)	$l(\lambda)\times10^6$ (Å^{-1}) (10*b*)	$L(\lambda)$ (10*c*)	$l\times10^6$ (Å^{-1}) (10*b*)	L (10*c*)
1.0	28.65	28.65	<1	28.65	179	28.65
2.0	14.34	14.34	<1	14.34	225	14.34
3.0	9.57	9.57	1	9.57	272	9.57
4.0	7.19	7.19	2	7.19	318	7.19
5.0	5.76	5.76	3	5.76	365	5.76
15.0	2.00	2.00	27	2.00	817	2.00
25.0	1.31	1.31	71	1.31	1211	1.31
35.0	1.06	1.06	131	1.06	1499	1.06
45.0	1.00	1.00	199	1.00	1646	1.00
55.0	1.06	1.06	267	1.06	1635	1.06
65.0	1.31	1.31	326	1.31	1466	1.31
75.0	2.00	2.00	371	2.00	1161	2.00
85.0	5.76	5.76	394	5.76	756	5.76
88.2	15.93	15.95	397	16.13	611	16.30
88.4	17.91	17.95	397	18.28	601	18.62
88.6	20.47	20.55	397	21.23	590	22.02
88.8	23.88	24.05	397	25.78	576	28.92
89.0	28.65	29.08	793	40.48	997	36.08
89.2	35.81	37.24	650	44.69	849	39.10
89.4	47.75	58.11	540	49.06	734	42.06
89.6	71.62	81.26	460	53.10	651	44.65
89.8	143.24	93.30	413	56.07	602	46.46
90.0	∞	98.68	397	57.18	585	47.12

(9*g*), the Lorentz factor

$$L(\varepsilon) = \Delta\theta_h(\varepsilon)/(2\varepsilon\lambda) \qquad (9h)$$

is obtained. Insertion of the approximation (3*c*) for $\Delta\theta_h(\varepsilon)$ results in

$$L \sim 1/(\sin 2\theta),$$

indicating that, for intermediate Bragg angles θ, (9*h*) corresponds to the commonly used Lorentz factor defined in (8*b*).

If the crystal is rotated with a constant angular velocity ω, the velocity of the reciprocal-lattice point (see the lower part of Fig. 3*c*) is $v = \omega d_h^*$. The component of this velocity in the radial direction is given by $v_{r^*} = \omega d_h^* \cos\theta = (\omega/\lambda)\sin 2\theta$. Only the similarity of the expression ω/v_{r^*} with (8*b*) justifies the somewhat misleading interpretation of the reciprocal value of v_{r^*} as an approximate measure (Buerger, 1960; Nuffield, 1966), for the dimensionless purely geometrical Lorentz factor, which is independent of the velocity of rotation as well as of the time t taken for the reciprocal-lattice point to pass through the reflection condition.

The values for the Lorentz factor (9*h*) of Cu $K\alpha_1$ radiation calculated for $r = 1.5$ μm are given in the third column of Table 2. They are compared with the familiar Lorentz factor $L = 1/\sin 2\theta_h$ given in the second column. Both Lorentz factors result in identical values for all Bragg angles, except for θ in the vicinity of $\pi/2$, where the commonly used Lorentz factor becomes infinite, whereas (9*h*) is finite everywhere.

The Lorentz factor in a real experiment. The geometrical conditions in reciprocal space for an intensity-profile measurement in a real experiment are depicted in Fig. 5(*b*). M, M_1 and M_2 are the centres of the Ewald spheres with radii r^*, r_1^* and r_2^* respectively. Sphere S_1, with the radius $r_1^* - \varepsilon$ and centre M_1, and sphere S_2, with radius $r_2^* + \varepsilon$ and centre M_2, are the limiting spheres of the region, where the reflection condition for an ideally perfect crystallite of the sample is fulfilled with respect to the central ray of a divergent incident beam. Because of the mosaicity of the sample and the divergence of the beam, the reciprocal-lattice point of the entire mosaic crystal is for the first time in a reflection position at point P_1' and for the last time at P_2'. For a real experiment, where $\Delta\lambda$, ε, δ and η are all nonzero, formulas (9*c*) must therefore be replaced by

$$\mathrm{d}l: l = \mathrm{d}\theta: \Delta\theta_h, \qquad (10a)$$

where the 'effective thickness' of the Ewald sphere in the direction of the reflected beam l corresponds to

$$l = P_1'M - P_2'M \qquad (10b)$$

and $\Delta\theta_h$ is defined in (6*a*). Following the reasoning of the previous subsection, the Lorentz factor for the real experiment can be expressed as

$$L = \Delta\theta_h/(l\lambda), \qquad (10c)$$

relating the generalized Lorentz factor to the peak width and 'effective thickness' of the Ewald sphere in the direction of the reflected beam. It is straightforward to calculate the 'effective thickness' of the Ewald sphere using the triangles $P_1'MO$ and $P_2'MO$ of Fig. 5(*b*). Results for the 'effective thickness' of the Ewald sphere l, using the parameters given in the headings of Tables 1 and 2, are given in the sixth column of Table 2. The proper generalized Lorentz factor is given in the seventh column of Table 2. For comparison, in columns four and five the appropriate values for $\varepsilon = \eta = \delta = 0$ and $\Delta\lambda/\lambda = 0.000306$ are given. In agreement with Figs. 3(*a*)-(*d*), l is constant ($=2\varepsilon$) if only the parameter ε is nonzero; l increases with increasing θ if only the wavelength spread is nonzero. In the case of a real experiment, l has a maximum for intermediate Bragg angles θ and a local maximum in the vicinity of $\theta = \pi/2$.

The generalized Lorentz factor is identical to the familiar one for nearly the whole region of possible Bragg angles, but it is finite in the vicinity of $\theta \sim 0$ or $\pi/2$ for all physically meaningful parameter combinations and the values depend on the parameters used for calculation.

It is obvious from Table 2 that, because of the equivalence between the familar and generalized Lorentz factor for most Bragg angles, the Lorentz

factor defined in (8*b*) is an excellent approximation for conventional Bragg scattering experiments, where the Bragg angle is rarely smaller than 5° or greater than 75°. But for the simulation of multiple-scattering events in ψ-scan patterns, the use not only of a new peak-width formula, analogous to (6*a*), but also of a generalized Lorentz factor, derived on the basis of (10*c*), is necessary, because angles making (8*a*, *b*) infinite are neither experimentally impossible nor unusual.

B. The 'integrated intensity' obtained during a θ–2θ–ψ scan

As pointed out in the *Introduction*, in multiple-scattering experiments, two rotations have to be considered: the rotation about the θ axis for a constant azimuth ψ and the rotation about the ψ axis at a constant angle θ.

(*a*) *Rotation about the θ axis*

1. *The width of the Umweganregung peak obtained during θ rotation*

Dependence of the peak width $\Delta\theta_{Umweg}$ on the radius of the ideally perfect crystallites and on the wavelength spread of the incident beam. Once more, it will first be assumed that the incident beam is exactly parallel and monochromatic and that the crystal is ideally perfect. In Figs. 6(*a*) and (*b*), the elevation and plan of Fig. 2 with respect to the direction of the θ axis are shown.

The width of the intensity profile of the operative reflection, $\Delta\theta_{op}$, is given by the angle $O_2'OO_1'$. In the case of double diffractiion, the reflected beam $\mathbf{s}_2$ ($\equiv MO'$) in Fig. 6(*a*) acts as incident beam for the cooperative reflection and consequently the point O' acts as the new zero point of the reciprocal lattice with respect to the cooperative lattice point. During the θ rotation about the point O, the new zero point O' moves along the trajectory $O_2'O_1'$. Simultaneously, the lattice point B, belonging to the cooperative reflection, moves along the trajectory B_2B_1. Because the reciprocal lattice is rotated as a whole ($OO'B$ is a rigid triangle), there is no independent rotation of the point B about the new zero point O'. The cooperative lattice point touches the 'thick' Ewald sphere for the first time not at B_2 but at B_3 and leaves it at B_4. The width of the intensity profile due to the cooperative reciprocal-lattice point B, $\Delta\theta_{coop}$, therefore corresponds to the angle B_3OB_4, *i.e.* $\Delta\theta_{coop}$ is equivalent to the peak width of the primary reflection, $\Delta\theta_{prim}$. It is obvious from Fig. 6(*b*) that, in the given example, not all of the intensity reflected in the MO' direction is reflected once more in the MB direction because, moving from B_2 to B_3 and from B_4 to B_1, the cooperative lattice point B is not in reflection position. The opposite can also be true: if the width $\Delta\theta_{op}$ is smaller than $\Delta\theta_{coop}$, then the cooperative reciprocal-lattice point is partly in a reflection position, but there is no incident intensity to be diffracted.

It will be assumed in the following that the intensity profile of both operative and cooperative reflections can be closely described by a Gaussian form, with standard deviations σ_{op} and σ_{coop}. These standard deviations are proportional to $\Delta\theta_{op}$ and $\Delta\theta_{coop}$ respectively. Both Gaussian distributions reach their maxima simultaneously at the same angle of rotation θ_0, at which both reciprocal-lattice points O' and B lie on the sphere S. The intensity profile of the double reflection is therefore given by

$$C_1 \exp[-\tfrac{1}{2}(\theta-\theta_0)^2/\sigma_{op}^2]\, C_2 \exp[-\tfrac{1}{2}(\theta-\theta_0)^2/\sigma_{coop}^2] = C \exp[-\tfrac{1}{2}(\theta-\theta_0)^2(\sigma_{op}^2+\sigma_{coop}^2)/(\sigma_{op}^2\sigma_{coop}^2)], \quad (11a)$$

where C_1, C_2 and C are constants. The peak width of the double reflection $\Delta\theta_{Umweg}$ will therefore be proportional to the standard deviation σ_{Umweg}, given by

$$\sigma_{Umweg} = \sigma_{op}\sigma_{coop}/(\sigma_{op}^2+\sigma_{coop}^2)^{1/2}. \quad (11b)$$

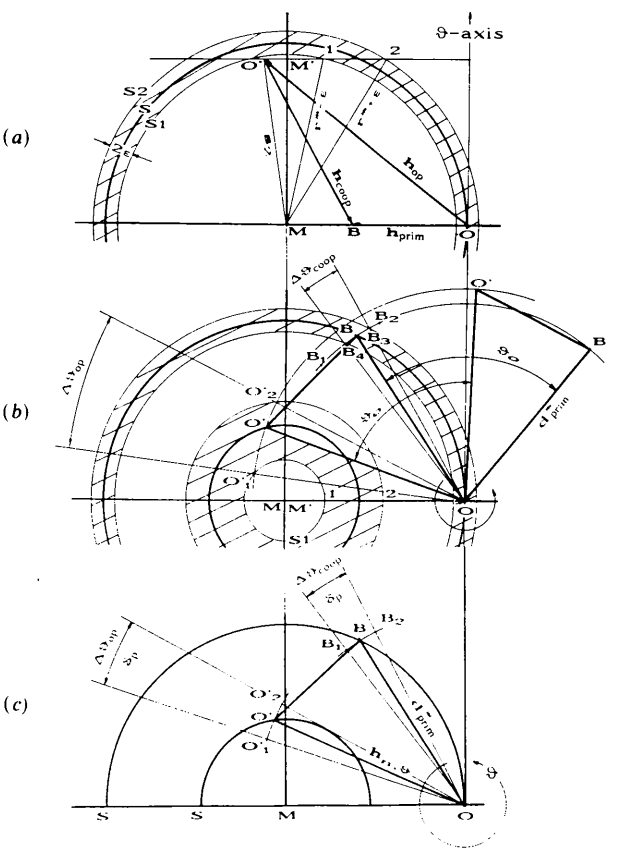

Fig. 6. Elevation and plan of the geometry in reciprocal space, given in Fig. 2, with respect to the direction of the θ axis. (*a*) Elevation with $\Delta\lambda = \delta = \eta = 0$, $\varepsilon \neq 0$. (*b*) Plan with $\Delta\lambda = \delta = \eta = 0$, $\varepsilon \neq 0$. (*c*) Plan with $\varepsilon = \Delta\lambda = 0$, $\delta \neq 0$, $\eta = 0$.

Table 3. *Comparison of measured and calculated peak widths (FWHM) of the forbidden* 003 *reflection of* Zn, *calculated for* Cu $K\alpha$

$\Delta\lambda/\lambda(\alpha_1) = 0.000301$, $\Delta\lambda/\lambda(\alpha_2) = 0.000413$, $\delta_p = 0.12°$, $\delta_s = 0.14°$, $r = 1/\varepsilon = 5$ μm, $\eta = 0.03°$, cell constants: $a = b = 2.6657$, $c = 4.9403$ Å, $\theta_{prim} = 27.89°$.

No.	$\mathbf{h}_{op}/\mathbf{h}_{coop}$	$\Delta\theta_{obs}$	$\Delta\theta_{Umweg}$	$\psi(\alpha_1/\alpha_2)$	$\Delta\psi_{obs}$	$\Delta\psi_{calc}$	$\Delta\psi_{Umweg}$
1	$\bar{2}0\bar{1}/204$	0.165 (5)	0.163	−37.99/−37.56	0.30 (1)	0.32 (1)	0.29
	$\bar{2}04/20\bar{1}$						0.30
2	$\bar{2}\bar{1}3/210$	0.165 (5)	0.163	−36.79/-	0.72 (2)	0.78 (2)	0.70
	$\bar{2}\bar{1}0/213$						0.92
3	$\bar{1}\bar{2}1/122$	0.162 (5)	0.163	−35.27/−35.76	0.30 (1)	0.30 (1)	0.27
	$\bar{1}\bar{2}2/121$						0.26
4	$0\bar{2}3/020$	0.168 (5)	0.163	−33.93/−34.14	0.35 (1)	0.36 (1)	0.24
	$0\bar{2}0/023$						0.23
5+5*a*	$\bar{1}11/1\bar{1}2$			−32.62/−32.58	0.25 (1)	0.23 (1)	0.22
	$\bar{1}12/1\bar{1}1$						0.24
6	$\bar{2}\bar{1}3/210$	0.165 (5)	0.163	−36.79/-	0.72 (2)	0.78 (2)	0.70
	$\bar{2}\bar{1}0/213$						0.92
7+7*a*	$0\bar{1}\bar{1}/014$			−29.91/−30.09	0.36 (1)	0.36 (1)	0.25
	$0\bar{1}4/01\bar{1}$						0.34
8	$0\bar{2}1/022$	0.168 (5)	0.163	−27.17/−27.33	0.32 (1)	0.31 (1)	0.22
	$0\bar{2}2/021$						0.22
9+9*a*	$\bar{1}13/1\bar{1}0$			−22.72/−22.65	0.25 (1)	0.25 (1)	0.28
	$\bar{1}10/1\bar{1}3$						0.21
10	$\bar{3}11/3\bar{1}2$	0.162 (5)	0.163	−16.32/−15.83	0.27 (1)	0.28 (1)	0.27
	$\bar{3}12/3\bar{1}1$						0.26

Drawing the appropriate Ewald construction, it can easily be shown that the considerations of this subsection also hold true for the dependence of the peak width on the wavelength spread of the incident beam.

Dependence of the peak width $\Delta\theta_{Umweg}$ on the divergence of the incident beam and on the mosaic spread of the crystal. In this subsection an infinite ideally perfect crystal and a negligibly small wavelength dispersion are assumed. As can be seen from Fig. 6(*c*), the peak widths of the operative and cooperative reflection, $\Delta\theta_{op}$ and $\Delta\theta_{coop}$, due to δ_p, the divergence of the incident beam in the scattering plane of the primary reflection, are equal to δ_p for all rotation angles θ, $\Delta\theta_{coop}$ being equal to $\Delta\theta_{prim}$. Furthermore, because the points B_2 and O_2' as well as the points B_1 and O_1' simultaneously touch the Ewald sphere, the same is true for the double diffraction,

$$\Delta\theta_{Umweg} = \delta_p. \tag{12}$$

In the last step, an exactly parallel and monochromatic incident beam and a crystal consisting of large mosaic blocks ($\varepsilon \sim 0$) will be considered. For an isotropic mosaic distribution, the mean angle between the reciprocal-lattice vectors, which belong to one reciprocal-lattice point, is constant for all directions and proportional to the mosaic spread η. Replacing the symbol δ_p in Fig. 6(*c*) by η_{max}, the largest angle between mosaic blocks, the vectors OB_1 and OB_2, for example, can be interpreted as the limiting vectors of possible $\mathbf{h}_{prim}$ in the plane of the paper. As long as one of the vectors $\mathbf{h}_{prim}$, lying between these two vectors, touches the Ewald sphere during rotation about the θ axis, the respective reciprocal-lattice point is in a reflection position. Because the three vectors $\mathbf{h}_{prim}$, $\mathbf{h}_{op}$ and $\mathbf{h}_{coop}$ form a rigid triangle and because the isotropic mosaic spread η is equal for all reciprocal-lattice vectors, it follows that, for the case when the conditions for double reflection are fulfilled, there is, for every $\mathbf{h}_{prim}$, the corresponding vector triangle $\mathbf{h}_{prim}$, $\mathbf{h}_{op}$ and $\mathbf{h}_{coop}$. Double diffraction therefore takes place as long as $\mathbf{h}_{prim}$ is in a reflection position, *i.e.*

$$\Delta\theta_{Umweg} = \eta. \tag{13}$$

The peak width in a real experiment. In a real experiment, the broadening of the Ewald sphere due to ε and $\Delta\lambda$ has to be considered simultaneously. The derivation of $\Delta\theta_{op}(\varepsilon, \Delta\lambda)$ and $\Delta\theta_{coop}(\varepsilon, \Delta\lambda)$ is straightforward using a 'thick' Ewald sphere similar to Figs. 6(*a*) and (*b*) that in addition takes into account the broadening due to $\Delta\lambda$.

Insertion of the full width at half-maximum (FWHM) for $\Delta\lambda$ and ε results in the relation

$$\sigma_{op,coop}(\varepsilon, \Delta\lambda) = \Delta\theta_{op,coop}(\varepsilon, \Delta\lambda)/(8 \ln 2)^{1/2} \tag{14}$$

between the peak width $\Delta\theta$ and the appropriate standard deviation of a Gaussian distribution. $\sigma_{Umweg}(\varepsilon, \Delta\lambda)$ can therefore be calculated using (11*b*). The peak width (FWHM) of the *Umweganregung* intensity profiles due to the ε, $\Delta\lambda$, δ and η (using FWHM for all four) is then given by

$$\Delta\theta_{Umweg} = \sigma_{Umweg}(\varepsilon, \Delta\lambda)(8 \ln 2)^{1/2} + \delta_p + \eta. \tag{15}$$

In Table 3, the calculated width $\Delta\theta_{Umweg}$ of the *Umweganregung* peaks of the forbidden 003 reflection of Zn are compared with the measured widths. The numbers given in the first column of Table 3 correspond to the appropriate peaks of Fig. 1(*a*), due to Cu $K\alpha_1$ radiation; the numbers followed by the letter '*a*' correspond to the same $\mathbf{h}_{op}/\mathbf{h}_{coop}$, but are due to Cu $K\alpha_2$ radiation. The peak width $\Delta\theta_{Umweg}$, given in the fourth column of Table 3, calculated for Cu $K\alpha_1$

radiation with parameters given in the heading of the table, agree very well with the observed ones, which are given in the third column of the table. This confirms the initially surprising fact, predicted in formula (15), that the widths $\Delta\theta_{\text{Umweg}}$ are nearly equal in magnitude for all *Umweganregung* peaks in the θ-2θ-ψ scan of the primary reflection under consideration. In Fig. 7, the triangle $O'OB$, defined in Fig. 6(b), for the *Umweganregung* peak number 2 is given in the correct proportion. In this case, the peak width $\Delta\theta_{\text{op}}$ of the operative reflection can be calculated to be 2.24°. This extremely high value is easily understood from Fig. 7. The peak width $\Delta\theta_{\text{coop}}$, on the other hand, can be calculated to be 0.163°, resulting in $\Delta\theta_{\text{Umweg}} = 0.163°$, in agreement with the experiment.

2. *The Lorentz factor for the θ rotation*

The 'effective thickness' l_{Umweg} of the Ewald sphere in the direction of the reflected beam can easily be deduced from Fig. 5(b), replacing $d_{\mathbf{h}}^*$ by d_{prim}^*, δ by δ_p and the lattice point P by the point B corresponding to the primary and cooperative reflection.

The simultaneous motion of reciprocal-lattice points B and O' (Fig. 6) about the θ axis results in the integrated intensity measured during the θ rotation being proportional to the Lorentz factor L_θ, given by

$$L_\theta = \Delta\theta_{\text{Umweg}}/(l_{\text{Umweg}}\lambda). \qquad (16)$$

Because of the dominant influence of the divergence δ_p on the peak width $\Delta\theta_{\text{Umweg}}$, if a conventional X-ray tube is used as source of the incident beam, the peak widths $\Delta\theta_{\text{Umweg}}$ are nearly equal in magnitude for all *Umweganregung* peaks in the θ-2θ-ψ scan of the primary reflection and are almost equal to the peak width $\Delta\theta_{\text{prim}}$. The Lorentz factor L_θ is therefore almost equal to $L_{\mathbf{h}_{\text{prim}}} = 1/(\sin 2\theta_{\text{prim}})$, for all *Umweganregung* peaks of the scan, being to a very good approximation $L_\theta = 1.21$ for all *Umweganregung* events of the forbidden 003 reflection of Zn depicted in Fig. 1. But it was shown by Bengel (1991) that L_θ given in (16) has to be taken into account in comparing *Umweganregung* intensities measured for different primary reflections.

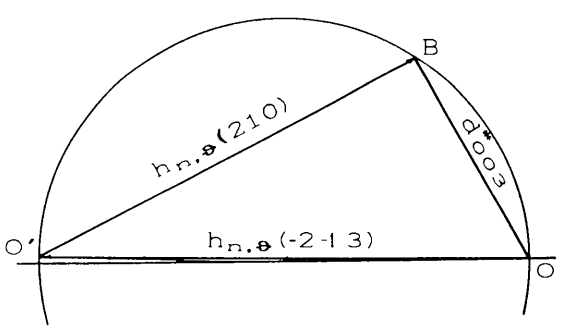

Fig. 7. Projection of the triangle of scattering vectors in correct proportion, corresponding to peak 2 in Fig. 1(a).

(b) *Rotation about the ψ axis*

1. *The width of the Umweganregung peak obtained during ψ rotation*

The multiple-scattering event during rotation about the ψ axis for the constant Bragg angle $\theta = \theta_{\text{prim}}$ is now considered. The peak width $\Delta\psi_{\text{Umweg}}$ depends on the parameters $\Delta\lambda$ and ε in a manner analogous to the peak width $\Delta\theta_{\text{Umweg}}$. However, the effect of δ and η on $\Delta\psi_{\text{Umweg}}$ differs from that on $\Delta\theta_{\text{Umweg}}$.

In Figs. 8(a) and (b), the elevation and plan of the geometry in reciprocal space, with respect to the direction of the ψ axis for a real experiment, are shown. Contrary to the condition during the θ rotation, the reciprocal-lattice point B belonging to the primary reflection as well as to the cooperative reflection does not move during ψ rotation. For $\theta = \theta_{\text{prim}}$ therefore, both reflections $\mathbf{h}_{\text{prim}}$ and $\mathbf{h}_{\text{coop}}$ remain in reflection position during the ψ rotation.

For the constant angle θ_{prim}, the effective divergence of the beam in the plane defined by the incident ray and the vector $\mathbf{h}_{\text{prim}}$ is limited by the angle $\delta_{p,\text{eff}}$ between the rays a and b (Fig. 8a). $\delta_{p,\text{eff}}$ is the smaller of the two angles δ_p and η, where δ_p is the divergence of the incident beam in the plane of Fig. 8(a). M in Fig. 8(a) is the centre of the sphere S with radius r^*. M_{1a}, M_{1b} are the centres of the spheres $S1a$, $S1b$, both with radius $r_1^* - \varepsilon$, and M_{2a}, M_{2b} are the centres of the spheres $S2a$, $S2b$, both with radius $r_2^* + \varepsilon$.

The peak width $\Delta\psi_{\text{op}}$ of the *Umweganregung* peak during ψ rotation can be deduced from Fig. 8(b) and is obviously given by

$$\Delta\psi_{\text{op}} = \beta_2 - \beta_1 + \delta_{s,\psi} + \eta_\psi^{\text{op}}, \qquad (17)$$

where η_ψ^{op} (Fig. 8c) is the angle of rotation in the plane normal to the ψ axis corresponding to the mosaic spread η. The divergence $\delta_{s,\psi}$, which depends on θ_{prim}, is defined in Fig. 8(d). Because $\mathbf{h}_{\text{coop}}$ is always in a reflection position during the rotation about the ψ axis, it follows from (11a, b) that $\Delta\psi_{\text{Umweg}}$ is determined solely by $\Delta\psi_{\text{op}}$,

$$\Delta\psi_{\text{Umweg}} = \Delta\psi_{\text{op}}. \qquad (18)$$

The values for $\Delta\psi_{\text{Umweg}}$, obtained using (17) and (18), for Cu $K\alpha_1$ are given in the eighth column of Table 3.

In Fig. 1(b), the measured intensity of the three-dimensional plot of Fig. 1(a), integrated over the θ scan, is plotted against ψ. In Table 3, the ψ values for the peak maxima of the *Umweganregung* peaks due to Cu $K\alpha_1$ and Cu $K\alpha_2$ are given in the fifth column. In the sixth column, the observed full widths at half-maxima, $\Delta\psi_{\text{obs}}$, of the intensity profiles 1 to 10 pictured in Fig. 1(b) are specified. Because of the overlapping of *Umweganregung* peaks due to $K\alpha_1$

and $K\alpha_2$ radiation in the example given in Fig. 1(*b*), it is not possible to compare the calculated peak width $\Delta\psi_{\text{Umweg}}$ directly with these measured ones. The utility of the peak width defined in (17) and (18) and the significance of $\Delta\psi_{\text{calc}}$, which is also given in Table 3, will become obvious in § III.1.

2. *The Lorentz factor for the ψ rotation*

As pointed out above, the lattice point B belonging to the primary as well as to the cooperative reflection is always in reflection position during rotation about the ψ axis. The intensity incident on the plane $\mathbf{h}_{\text{coop}}$ during the ψ rotation is therefore identical to the integrated intensity reflected by $\mathbf{h}_{\text{op}}$. Consequently, the integrated intensity reflected by $\mathbf{h}_{\text{coop}}$ is proportional to L_ψ defined as

$$L_\psi = \Delta\psi_{\text{op}}/(l_{\text{op},\psi}\lambda). \qquad (19a)$$

From Figs. 8(*a*) and (*b*) it can be deduced that $l_{\text{op},\psi}$ is given approximately by

$$l_{\text{op},\psi} = |MO_2' - MO_1'|. \qquad (19b)$$

In Table 4, L_ψ calculated using (19*a*) is compared with L_ψ defined by (8*a*), for some of the *Umwegan-regung* events of Fig. 1(*b*). From Fig. 2 and Figs. 8(*a*) and (*b*), it can easily be deduced that L_ψ defined by (8*a*) can be expressed as

$$L_\psi = 1/[\lambda h_{n,\psi}(\cos\theta_{\text{prim}})(\sin\beta)]. \qquad (19c)$$

Apart from the factor $1/\lambda$, (19*c*) corresponds to the Lorentz factor L_ψ given by Post (1975). The results obtained for (8*a*), *i.e.* (19*c*), are given in the fifth column of Table 4. The appropriate values for $h_{n,\psi}$ and β are also given in Table 4. In the sixth column, the peak width $\Delta\psi_{\text{op}}$ is specified in degrees; in (19*a*) it has to be specified in radians. In the seventh and

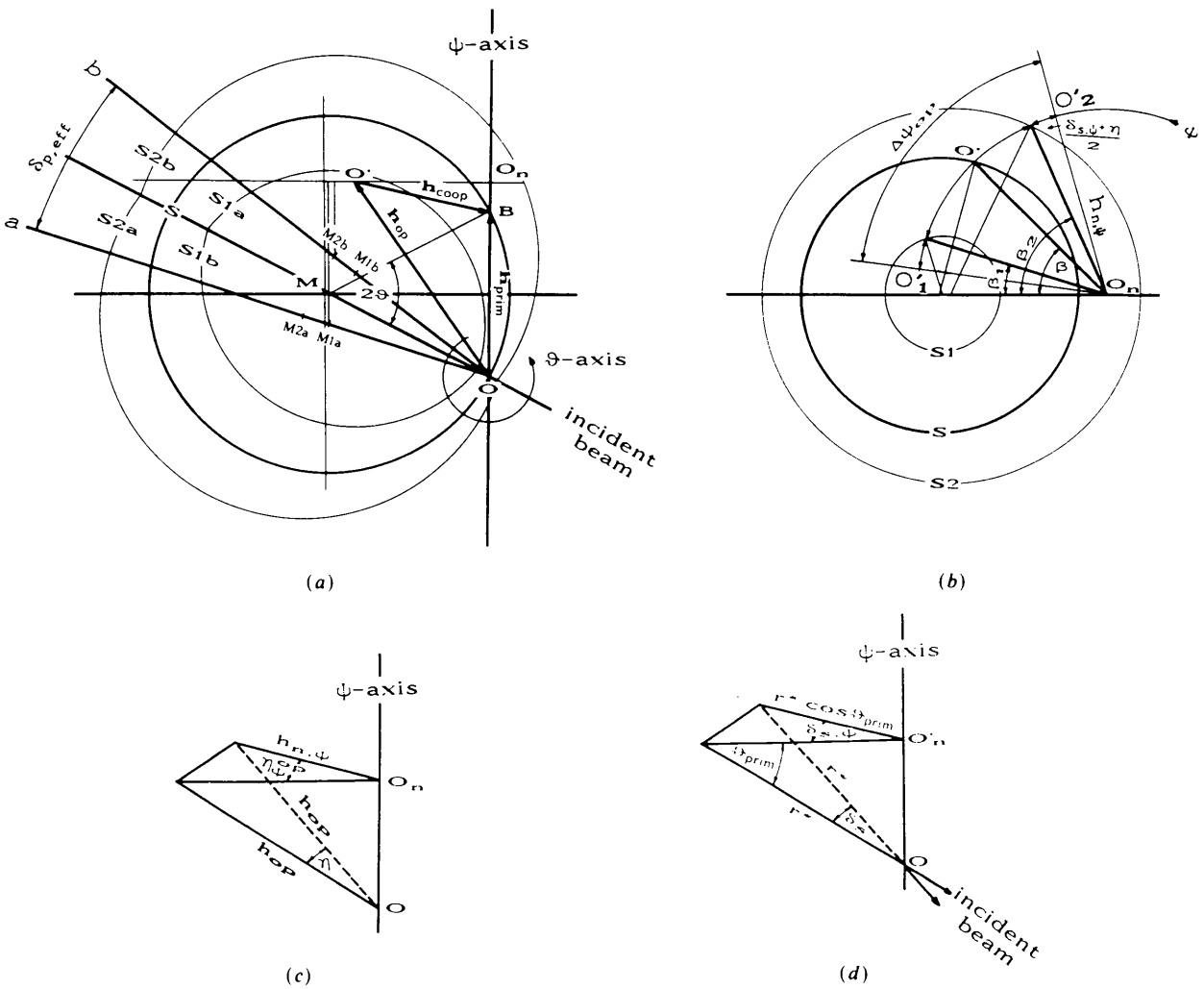

Fig. 8. The geometry in reciprocal space, given in Fig. 2, with respect to the direction of the ψ axis. Real experiment. (*a*) Elevation. (*b*) Plan. Trajectory of the operative reciprocal-lattice point. (*c*) Definition of η_ψ^{op}. (*d*) Definition of $\delta_{s,\psi}$.

Table 4. *The Lorentz factors L_ψ and L_θ for the Umweganregung events of Fig. 1(b) of the forbidden 003 reflection of* Zn, *calculated for* Cu $K\alpha_1$ *with the parameters given in Table 1*

No.	$\mathbf{h}_{op}/\mathbf{h}_{coop}$	$h_{n,\psi}$ (Å^{-1})	β (°)	L_ψ (19c)	$\Delta\psi_{op}$ (°)	l_{op} $\times 10^6$ (Å^{-1})	L_ψ (19a)
1	$\bar{2}0\bar{1}/204$	0.866	23.09	2.16	0.2870	1504	2.16
2	$2\bar{1}0/213$	1.1461	2.78	13.20	0.9230	785	13.32
3	$\bar{1}\bar{2}1/122$	1.1461	20.53	1.83	0.2733	1694	1.83
4	$0\bar{2}3/020$	0.866	40.97	1.29	0.2430	2129	1.29
5	$\bar{1}11/1\bar{1}2$	0.433	77.72	1.74	0.2166	1415	1.74
7	$0\bar{1}\bar{1}/014$	0.433	44.99	2.40	0.2469	1166	2.40
8	$0\bar{2}1/022$	0.866	47.73	1.15	0.2168	2144	1.15
9	$\bar{1}13/1\bar{1}0$	0.433	67.82	1.83	0.2763	1710	1.83
10	$\bar{3}11/3\bar{1}2$	1.146	20.53	1.83	0.2733	1694	1.83

eighth columns l_{op} and L_ψ, defined in (19*b*) and (19*a*), are given. The generalized Lorentz factor introduced in this paper is identical to that given by Post (1975) for *Umweganregung* peaks except for peak 2, for which the angle β is near zero.

The advantage of the generalized Lorentz factor is that it is - in contrast to Post's - finite for $\beta = 0$ or π, and that it is very sensitive to the parameters $\Delta\lambda$, δ, ε and η used for calculation in the vicinity of these angles.

III. Experimental check of the proposed peak widths and Lorentz factors: comparison between measured and calculated *Umweganregung* patterns

In the program *UMWEG*90, the new peak widths and Lorentz factors introduced in this paper are used for the calculation of the intensities defined in (1*a-e*). The advantages of the new expressions for $\Delta\theta$, $\Delta\psi$, l, L_θ and L_ψ are that they are finite everywhere, that they depend on the parameters $\Delta\lambda$, δ, ε and η in a distinct manner and that they are very sensitive to parameter changes in the vicinity of angles for which the formulae usually used become infinite. Two examples of the successful application of the concepts introduced in this paper will be given below.

1. *The Umweganregung pattern of the forbidden* 003 *reflection of* Zn

In Fig. 1(*c*), the simulation of the measured *Umweganregung* pattern of Fig. 1(*b*), calculated with *UMWEG*90 is given. The parameters used for the calculation are given in the legend of the figure. The full widths at half-maxima $\Delta\psi_{obs}$ and $\Delta\psi_{calc}$ of the intensity profiles 1 to 10 pictured in Figs. 1(*b*) and (*c*) are specified in Table 3. For each wavelength, Cu $K\alpha_1$ as well as Cu $K\alpha_2$, the profiles of all these peaks are due to the overlapping of two *Umweganregung* events. The agreement between the two patterns is excellent, bearing in mind the possible errors due to the measurement (see Fig. 1 of Rossmanith, 1986) and the simplicity of the isotropic mosaic structure model used. The greatest deviation between measurement and calculation is found for peak 5, which is due to two strong reflections. The deviation may therefore, in addition, be due to extinction as well as absorption effects, which have been neglected in *UMWEG*90 until now.

Peaks 2 and 6 in particular in Fig. 1(*b*) are not symmetrical. This is readily understood from Fig. 8(*b*). The angle β for these peaks is small (see Table 4). The angle $O_2'O_nO'$ is smaller than the angle $O'O_nO_1'$. In O' the maximum of the peak is reached. To take this fact into account, the peak profile is simulated in the program *UMWEG*90 by combining two Gaussian distributions with two different standard deviations σ_1 and σ_2 for the two halves of the distribution

$$\sigma_1 = (\beta_2 - \beta + \delta_{s,\psi} + \eta_\psi^{op})/(8 \ln 2)^{1/2}, \quad (20a)$$

$$\sigma_2 = (\beta - \beta_1 + \delta_{s,\psi} + \eta_\psi^{op})/(8 \ln 2)^{1/2}. \quad (20b)$$

For joining the two halves at the same maximum value, the normalization factor in (1*b*, *c*) is replaced by

$$(8\pi)^{-1/2}(1/\sigma_1 + 1/\sigma_2). \quad (20c)$$

The asymmetry of peaks 2 and 6 of Fig. 1(*c*) is satisfactorily predicted by the program *UMWEG*90. Future implementation of alternative theoretical distributions will probably result in even better agreement.

2. *The Umweganregung pattern of the forbidden* 222 *reflection of diamond*

The first *Umweganregung* pattern was given by Renninger (1937). In Fig. 9(*a*) a copy of his famous '*Azimutregistrierung der Reflexionsintensität von Diamant* (222)' is given. The figure shows the pattern for a 360° rotation about the scattering vector of the

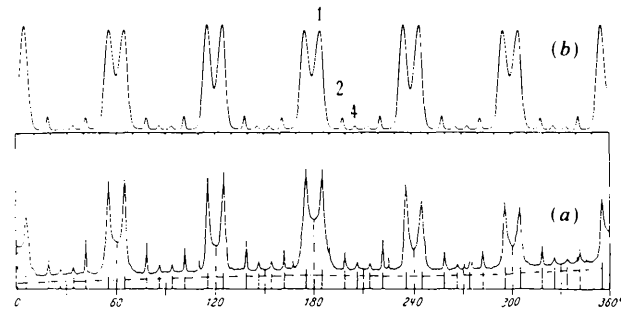

Fig. 9. *Umweganregung* pattern of the 222 reflection of diamond. (*a*) '*Azimutregistrierung der Reflexionsintensität von Diamant* (222)' - copy of Fig. 2 given by Renninger (1937). Cu $K\alpha$. (*b*) Calculation by *UMWEG*90. Cu $K\alpha$. Cell constants: $a = 3.5667$ Å; temperature parameters: $\beta_{ii} = 0.0016$, $\beta_{ij} = 0$; atomic scattering factors for C: Table 2.2*B*, *International Tables for X-ray Crystallography* (1974); $\Delta\lambda/\lambda$ as before; $\delta_s = \delta_p = 1°$; $\eta = 0.18°$; $r = 5$ μm; GL = 0.1.

'almost forbidden' 222 reflection, obtained with Cu $K\alpha$ radiation. The divergence δ of the incident beam in Renninger's experiment was between 0.5 and 1° and the mosaic spread (*Reflexionswinkelbereich*) of different samples varied between a few angular seconds and 1°.

The extraordinary width of peak 1 in Fig. 9 is due to the relatively small angle β. The corresponding reciprocal-lattice point enters and leaves the $K\alpha_1$ Ewald sphere within 9.56° and does not touch the $K\alpha_2$ sphere at all. The Lorentz factor for the ψ rotation, defined in (19*c*) and given in Table 5 together with $h_{n,\psi}$ and the angle β, is therefore large.

The absence of peak 3 (see Table 5) in his pattern was explained by Renninger to be due to the very small value of the polarization factor p_{12}.

If one bears in mind that $\Delta\theta_{\text{Umweg}}$ is almost equivalent for all the peaks in one ψ scan and equal to $\Delta\theta_{\text{prim}}$, the additional factor in (1*e*) can be incorporated in the scale factor. The additional factor has to be taken into consideration if synchrotron radiation with its characteristic small divergence is used. In this case, the widths $\Delta\theta_{\text{Umweg}}$ may differ appreciably for different peaks.

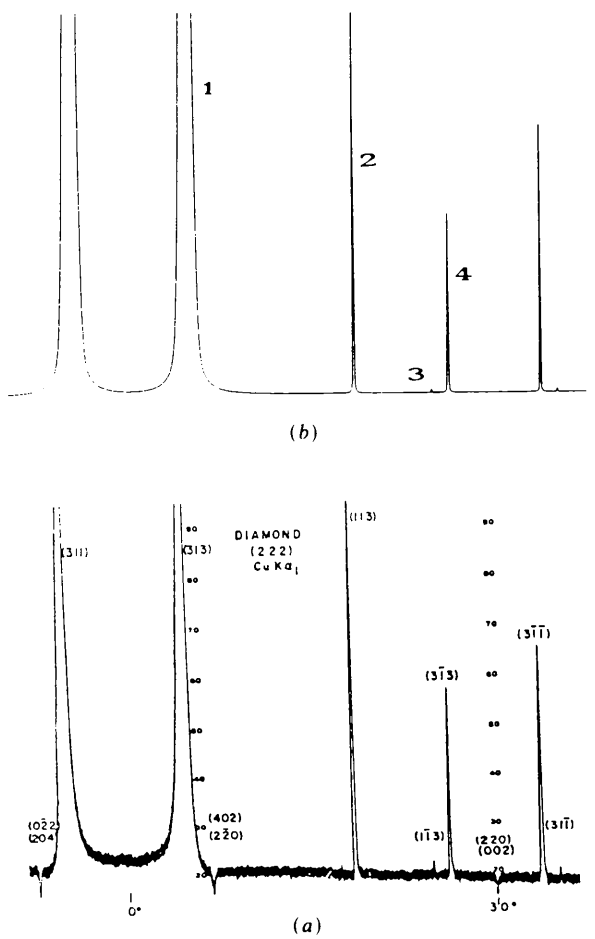

Fig. 10. *Umweganregung* pattern of the 222 reflection of diamond. (*a*) Measurement by Post (1976). Cu $K\alpha_1$. (*b*) Calculation by *UMWEG*90. Cu $K\alpha_1$. $\delta_s = \delta_p = 0.01°$; $\eta = 0.001°$; $r = 100$ μm; GL = 0.2; remaining parameters as in Fig. 9(*b*).

In Fig. 9(*b*) the simulation calculated with *UMWEG*90 using $\delta_s = \delta_p = 1°$ and $\eta = 0.18°$ is given. The divergence and the mosaic spread were fitted, within the limits stated by Renninger, to give the best agreement between measurement and calculation. The parameters used for calculation are given in the legend of the figure. The calculation with *UMWEG*90 predicts the Renninger pattern surprisingly well.

A 30° portion of the diamond 222 pattern was recorded once more with improved resolution by Post (1976). The divergence of the incident beam was limited to $\delta \leq 0.033°$. Post reports in his paper that the divergence exceeded the acceptance angles of the interactions and that therefore integrated intensities were measured in the scanning process with standard errors of 40%. The copy of Post's pattern, given in Fig. 10(*a*), is compared with the simulation in Fig. 10(*b*), calculated with parameters fitted within the limits given by Post to give the best agreement between the measured and calculated patterns. The value obtained for the FWHM of $\delta_s = \delta_p = 0.01°$ agrees well with the divergence in the experiment, whose maximum was limited to 0.03°. The very small peak 3 can be observed in the measured as well as in the calculated drawings.

To get better agreement between measured and calculated intensity profiles, the exponential function in (1*c*, *e*) is replaced by

$$(1-\text{GL})\exp\{-\tfrac{1}{2}(\psi_i-\psi_{\text{op}})^2/\sigma_{\text{op}}^2\} + \text{GL}\{1+[2(\psi_i-\psi_{\text{op}})/\Delta\psi_{\text{op}}]^2\}^{-1} \qquad (21)$$

in the program *UMWEG*90. GL is a measure for the Lorentzian contribution to the theoretical distribution.

A very good fit of the intensity profile of peak 1 was obtained using 20% Lorentzian contribution to the theoretical distribution instead of the 10% used in Fig. 9(*b*). This can be readily explained: the width of this peak is mainly due to wavelength dispersion, $\varepsilon = 1/r = 1/100$ μm and $\eta = 0.001°$ are very small in this fit.

In Table 5, the Lorentz factors L_ψ, calculated with the different parameter sets, used for calculation of the patterns of Figs. 9(*b*) and 10(*b*), are also given. Apart from peak 1, these factors are identical to the familiar one. However, for β in the vicinity of zero, the new Lorentz factor deviates from that given by Zachariasen (1945), the deviation being dependent on the parameter set used.

The intensity of the peak 1 calculated with (1*c*, *e*) is very sensitive to the values obtained for L_ψ as well as for the peak width σ_{op}. Because both quantities

Table 5. *Comparison of the Lorentz factors L_ψ defined in (23a) and (23b) for the Umweganregung events of the 'almost forbidden' 222 reflection of diamond, marked in Figs. 9 and 10, calculated for* Cu $K\alpha_1$ *with* $\Delta\lambda/\lambda(\alpha_1) = 0.000301$

Cell constant: $a = 3.5667$ Å, $\theta_{prim} = 48.43°$.
$L_\psi(P)$: $\delta_p = \delta_s = 0.01°$, $r = 100$ μm, $\eta = 0.001°$, corresponding to Fig. 10(*b*).
$L_\psi(R)$: $\delta_p = \delta_s = 1°$, $r = 5$ μm, $\eta = 0.18°$ corresponding to Fig. 9(*b*).

No.	$\mathbf{h}_{op}/\mathbf{h}_{coop}$	$h_{n,\psi}$ (Å^{-1})	β (°)	L_ψ (19*c*)	$L_\psi(P)$ (19*a*)	$L_\psi(R)$ (19*a*)
1	$313/\bar{1}1\bar{1}$	0.458	4.78	25.65	25.74	28.61
2	$113/11\bar{1}$	0.458	78.50	2.18	2.18	2.18
3	$1\bar{1}3/13\bar{1}$	0.793	54.88	1.51	1.51	1.51
4	$3\bar{1}3/\bar{1}3\bar{1}$	0.916	26.25	2.42	2.42	2.42

depend on the four parameters $\Delta\lambda$, δ, ε and η in a distinct manner, *UMWEG*90 is an efficient tool for the determination of the divergence and wavelength spread of the incident beam as well as of the mosaic spread and block size in the sample.

Furthermore, Figs. 1(*b*), (*c*), 9(*a*), (*b*) and 10(*a*), (*b*) demonstrate the ability of *UMWEG*90 to predict the *Umweganregung* patterns for measurements carried out under very different experimental conditions.

References

AZAROFF, L. V. (1968). *Elements of X-ray Crystallography.* New York: McGraw-Hill.
BENGEL, K. (1991). Diplomarbeit, Univ. Hamburg, Germany.
BUERGER, M. J. (1960). *Crystal-Structure Analysis* pp. 40-46. New York: John Wiley.
COMPTON, A. H. & ALLISON, S. K. (1935). *X-rays in Theory and Experiment.* Princeton, New Jersey: van Nostrand.
Enraf-Nonius (1982). *CAD-4 User's Manual.* Enraf-Nonius, Delft, The Netherlands.
FURNAS, T. C. (1957). *Single-Crystal-Orienter Instruction Manual.* Milwaukee: General Electric Company.
International Tables for X-ray Crystallography (1974). Vol. IV. Birmingham: Kynoch Press. (Present distributor Kluwer Academic Publishers, Dordrecht.)
JAMES, R. W. (1948). *The Optical Principles of the Diffraction of X-rays.* London: Bell.
LADELL, J., ZAGOFSKY, A. & PEARLMAN, S. (1975). *J. Appl. Cryst.* **8**, 499-506.
LAUE, M. (1960). *Röntgenstrahlinterferenzen.* Frankfurt am Main: Akademische Verlagsgesellschaft.
NUFFIELD, E. W. (1966). *X-ray Diffraction Methods*, pp. 72-73. New York, London, Sydney: John Wiley.
POST, B. B. (1975). *J. Appl. Cryst.* **8**, 452-456.
POST, B. (1976). *Acta Cryst.* A**32**, 292-296.
RENNINGER, M. (1937). *Z. Phys.* **106**, 141-176.
ROSSMANITH, E. (1986). *Acta Cryst.* A**42**, 344-348.
WÖLFEL, E. R. (1975). *Theorie und Praxis der Röntgenstrukturanalyse.* Braunschweig: Friedrich Vieweg.
ZACHARIASEN, W. H. (1945). *Theory of X-ray Diffraction in Crystals*, pp. 99-108. New York: John Wiley.
ZACHARIASEN, W. H. (1965). *Acta Cryst.* **18**, 705-710.

Acta Cryst. (1992). A**48**, 610-618

Refinement of Incommensurate Structures against Diffraction Data from a Twinned Crystal

BY SANDER VAN SMAALEN

Laboratory of Chemical Physics, Materials Science Centre, University of Groningen, NL9747 AG Groningen, The Netherlands

AND VÁCLAV PETŘÍČEK

Institute of Physics, Czechoslovak Academy of Sciences, Cukrovarnicka 10, 162 00 *Praha* 6, *Czechoslovakia*

(*Received* 19 *December* 1991; *accepted* 6 *February* 1992)

Abstract

Twinning can lead to a diffraction pattern with additional reflections that are incommensurate with the reflections of a crystal with only one orientation of the structure. The integer indexing of such a diffraction pattern involves more than three reciprocal-basis vectors. Analogously, for incommensurate crystals, the original number of $(3+d)$ reciprocal vectors should be extended to a larger set for a twinned incommensurate crystal. In this paper, it is shown that the diffraction symmetry for a twinned crystal can be analyzed in a way analogous to the treatment of the symmetry of an incommensurate structure. The theory is implemented in a refinement program for X-ray and neutron diffraction data and allows all intensity data from isolated and overlapping reflections to be taken into account. The method can also be applied to the refinement of ordinary crystal structures. The program has been used to determine the modulated structure of the inorganic misfit layer compound $(HoS)_{1.23}NbS_2$.

0108-7673/92/040610-09$06.00